PCCP

Accepted Manuscript

ROYAL SOCIETY OF CHEMISTRY

www.rsc.org/pccp

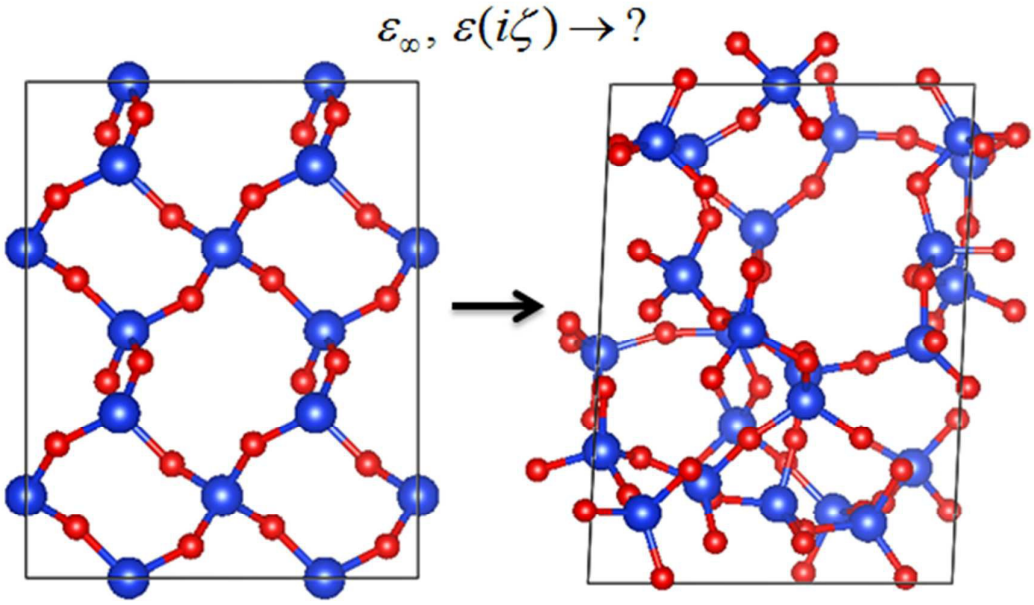

Dielectric properties of amorphous SiO_2 are other SiO_2 polymorphs are linked by simple volume dependence.

Volume dependence of dielectric properties of amorphous SiO_2

Oleksandr I. Malyi[1]*, Mathias Boström[1], Vadym V. Kulish[2], Priyadarshini Thiyam[3], Drew F. Parsons[4], and Clas Persson[1,3,5]

1 – Centre for Materials Science and Nanotechnology, University of Oslo, P. O. Box 1048 Blindern, NO-0316 Oslo, Norway

2 – Department of Mechanical Engineering, National University of Singapore, Block EA #07-08, 9 Engineering Drive 1, Singapore 117576, Singapore

3 – Department of Materials Science and Engineering, Royal Institute of Technology, SE-100 44 Stockholm, Sweden

4 – School of Engineering and Information Technology, Murdoch University, 90 South St, Murdoch, WA 6150, Australia

5 – Department of Physics, University of Oslo, P. O. Box 1048 Blindern, NO-0316 Oslo, Norway

Email: oleksandr.malyi@smn.uio.no (O.I.M*)

Abstract

Using first principles calculations, the analysis of dielectric properties of amorphous SiO_2 (am-SiO_2) was performed. We found that the am-SiO_2 properties are volume dependent, and the dependence is mainly induced by the variation of nanoporosity at atomic scale. In particular, both ionic and electronic contributions to the static dielectric constants are functions of volume with clear trends. Moreover, using unique parametrization of the dielectric function provided in this work, we predict dielectric functions at imaginary frequencies of different SiO_2 polymorphs having similar band gap energies.

Keywords: dielectric properties, amorphous SiO_2, first principles calculations, volume dependence, Born–Oppenheimer molecular dynamics

Introduction

SiO_2 is one of the most abundant materials and has been intensively studied during the last decades. It is well known that alpha quartz (α-SiO_2) is the equilibrium SiO_2 polymorph at room temperature, and that it has an indirect band gap with the gap energy of about 9 eV.[1-4] Due to unique structural properties of SiO_2 materials, it is possible to realize highly stable amorphous SiO_2 (am-SiO_2) consisting of a number of SiO_4 tetrahedra linked in a network.[5, 6] The tetrahedra have the possibility to rearrange and stabilize different porous structures. As an illustration, Zhao *et al.* synthesized a mesoporous SiO_2 with periodic 50 to 300 Å pores.[7] Indeed, the ability to optimize the size of Si-O rings allows am-SiO_2 to avoid large lattice mismatch at the interface with other materials making it attractive for application in semiconductor industry. Moreover, porous am-SiO_2 can be used for different applications from catalysis to controlled drug release, where the pores can play a dominant role.[8] Because of these, a number of experimental works were focused on synthesis and engineering of different am-SiO_2 systems. [7, 9, 10] Theoretical works had also a noticeable contribution to understanding of structural, electronic, and optical properties of am-SiO_2.[5, 6, 11-14] However, as amorphous solids do not have well defined structures, and am-SiO_2 properties are highly sensitive to the conditions under which the samples are synthesized/generated, both experimental and theoretical results differ noticeably from system to system. This can be partially induced by variation of material density. Since it is difficult to control amorphous structures experimentally, to the best of our knowledge, there is still no understanding of the am-SiO_2 properties as a function of its volume and their link to those of other SiO_2 polymorphs. Because of this, in this work, we combine both first principles "static" density functional theory (DFT) calculations and Born–Oppenheimer molecular dynamics (BOMD) simulations to analyze am-SiO_2 and other SiO_2 polymorphs.

Methods

All calculations are carried out using the Vienna Ab initio Simulation Package (VASP). The exchange-correlation term is described using the Perdew-Burke-Ernzerhof (PBE)[15] functional. Projector augmented wave (PAW) pseudopotentials[16, 17] are used to model the effect of core electrons. The non-local parts of the pseudopotentials are treated in reciprocal and real space for final "static" DFT calculations and BOMD simulations, respectively. After tests, the cutoff energies for plane-wave basis are set to 600, 400, and 300 eV for optimization of lattice parameters, final "static" DFT calculations, and BOMD simulations, respectively. The Brillouin-zone integrations are performed using the Γ-centered Monkhorst-Pack[18] grids of different sizes (see Table S1). All atoms are relaxed until the internal forces are smaller than 0.01 eV/Å. We use canonical ensemble BOMD simulations with the Nosé thermostat[19, 20] and time step of 1-1.5 fs to generate am-SiO_2 samples. To analyze dielectric properties of SiO_2 materials, for each system, the complex dielectric function $\varepsilon(\omega) = \varepsilon_1(\omega) + i\varepsilon_2(\omega)$ is computed. Here the imaginary part of the dielectric function ($\varepsilon_2(\omega)$) is calculated from the joint density of states as discussed elsewhere[21], while the real part of the dielectric function ($\varepsilon_1(\omega)$) and dielectric function at imaginary frequencies ($\varepsilon(i\zeta)$) are obtained from the Kramers–Kronig transformation. The static dielectric constant (ε_0) is taken as $\varepsilon_0 = \varepsilon_\infty + \chi$, where ε_∞ and χ are high frequency dielectric constant and ionic contribution to ε_0, respectively. χ is computed using the density functional perturbation theory.[22]

Results and discussion

Due to the high SiO_2 melting temperature, to generate am-SiO_2 structures a two-step temperature protocol is used (see Fig. 1a). First, at temperature about 5000 K, the samples are melted for a period of 10 ps. The obtained systems are then quenched to 2500 K during 5-25

ps and further annealed for the period of 10-20 ps at 2500 K. Finally, the obtained samples are quenched to 1 K for a period of 25-30 ps. It should also be noted that we perform a few different tests (e.g. different quenching rates, different annealing time) to ensure that formation of highly energetically unfavorable defect configurations (e.g. 2-membered Si-O rings) is not observed in am-SiO_2. The methodology used to generate amorphous structures is similar to that used in previous works.[5, 6, 12] To have a variety of am-SiO_2 structures, for the BOMD simulations, we vary the initial system volume within 7 % of the equilibrium α-SiO_2 value by changing c/a ratio of the lattice constants. In total, 10 different am-SiO_2 systems are generated with a volume spread of about 8%. A typical radial distribution function of am-SiO_2 shown in Fig. 1b is consistent with that reported by other groups.[13, 14] Similar to α-SiO_2, for all am-SiO_2 samples, all Si atoms are 4-coordinated and the stability of the material is therefore determined by polar covalent bonds. The average am-SiO_2 band gap energy is 5.3 eV, while for α-SiO_2 it is 5.7 eV. Although the PBE gap energies are smaller than the experimental ones, the observed reduction due to amorphization is consistent with previously reported data.[11, 23] It should be noted that am-SiO_2 band gap energy increases from about 5.2 eV for the densest sample to about 5.5 eV for the lowest density one, and this effect is opposite to that for α-SiO_2 (see Fig. 2). Because of this, we believe that it is mainly induced by formation of totally new amorphous structure-optimization of Si-O rings. As an illustration, despite the difference in the volumes, the average Si-O bond length for all amorphous samples is 1.633±0.003 Å (see Table 1). Although the dependence of am-SiO_2 electronic properties on its volume was not reported before, the variation of am-SiO_2 band gap energies is within the accuracy of the reported experimental data.[24]

Since PBE calculations underestimate the band gap energy, to reproduce the experimental value of 8.9±0.2 eV[24] and describe dielectric properties accurately, we use the scissors-operator approximation with Δ = 3.6 eV for shifting the conduction bands. Such an

approach has been widely tested to analyze the dielectric properties of materials and has proved to provide reliable results.[13, 25] Moreover, with Δ = 3.6 eV, ε_∞ is 2.2 and 2.1 for α-SiO_2 and am-SiO_2 (for am-SiO_2, the average value over the samples is given), respectively, while the corresponding experimental data are 2.2-2.3 and 2.1.[14, 26-28] The results are also in good agreement with other theoretical investigations reporting the values from 2.0 to 2.2.[13, 14]

The frequency dependent dielectric tensors of the am-SiO_2 samples are anisotropic (see Fig. S1). However, as the difference in the diagonal tensor components is minor, to simplify further discussion, the average value of *xx*, *yy*, and *zz* tensor elements of each sample is used. The dielectric functions for the am-SiO_2 structures shown in Fig. 3 are similar. In particular, for each sample, $\varepsilon_1(\omega)$ has a maximum and minimum at about 12 and 23 eV, respectively. At fixed frequencies before the maximum, $\varepsilon_1(\omega)$ is a function of inverse volume (V^{-1}). The difference between $\varepsilon_1(\omega)$ of different samples reduces near the maximum. For frequencies above the maximum, the difference in $\varepsilon_1(\omega)$ is small and cannot be clearly defined. To better understand this observation, we analyze ε_∞ which has a clear volume dependence (see Fig. 4a). Taking into account that the am-SiO_2 band gap energy is a function of the volume (see Fig. 2), it can be wrongly assumed that the dependence of ε_∞ is caused by different electronic properties of the am-SiO_2 samples. Indeed, it is well known that the increase in band gap energy, for instance via application of Δ correction, reduces ε_∞ of the material. Nevertheless, the use of different Δ values to tune am-SiO_2 band gap energy of each sample to 8.9 eV still indicates that the band gap dependence has only a minor effect on ε_∞ (see Fig. 4a). Because of this, we believe that the dependence of ε_∞ can be attributed directly to the volume effect.

It is well known that dielectric properties of a material depend on porosity. Moreover, a few models of the effect of mesoporosity on effective optical properties of a material have

been reported.[29-31] Among the approaches, the volume averaging theory (VAT) was shown to provide an accurate description of the dielectric constant of mesoporous SiO_2.[29-31] For the VAT model, the effective dielectric constant of a porous material (ε_{eff}) with vacuum pores is calculated as a function of porosity (ϕ) and the dielectric constant of continuous phase (ε_c) as $\varepsilon_{eff} = (1-\phi)\varepsilon_c + \phi$. Recently, it was also shown that ε_∞ of a 2-dimensional slab has V^{-1} dependence, and it is common to use this dependence in first principles analysis of defect stability in 2-dimensional materials.[32] In this work, we prove that the expanded VAT model can be used at an atomic level when classical definition of porosity is applied. If the system volume (V) is the sum of crystalline (V_c) and porous (V_p) volumes and V_c does not change from sample to sample, it is easy to see that the VAT model provides V^{-1} dependence as $\varepsilon_{eff} = \frac{V_c}{V}\varepsilon_c + 1 - \frac{V_c}{V}$. Calculating V_c using the Slater's Si and O atomic radii[33], ε_∞ can be fitted as a function of volume (see Fig. 4b). The found dependence can also be used to predict dielectric constants for other SiO_2 polymorphs with high accuracy. In Fig. 4b, we show the VAT extrapolation of the am-SiO_2 data and ε_∞ values for different SiO_2 polymorphs having PBE bandgaps from 5.2 to 5.7 eV. One should note that for all systems Δ = 3.6 eV is applied. This is indeed a fundamental observation as it indicates that the dielectric constant of the material is directly linked to its volume. Moreover, it is easy to see that the expanded VAT model will transform to the classical VAT model for mesoporosity. Here the model is proven to work well for the materials with similar band gap energies. However, it is obvious that the proposed method will not be able to describe materials that have a huge difference in the electronic properties or semiconductor-metal transition. In particular, the strain effect on ε_∞ is not expected to be well described using the VAT model, which is mainly due the dependence of band gap on stress. The model may also have a limitation for the analysis of low-band gap

materials where even minor change in the band gap energy can affect the dielectric properties noticeably.

Similar to ε_∞, χ is also volume dependent. Indeed, it is not surprising as $\chi \propto V^{-1}$ by definition.[22] For am-SiO_2, χ reduces from 2.14 for the densest sample to 1.81 for the lowest density one (see Table 1). Here average ε_0 computed over the am-SiO_2 samples is 4.05, which is in good agreement with previously reported data.[34-36] Although am-SiO_2 data can be fitted as function of V^{-1} (see Fig. 5), the dependence cannot be well extrapolated for all SiO_2 polymorphs. We believe that it is due to sensitivity of vibration frequencies used in calculations of χ to the volume changes. Moreover, for the densest SiO_2 polymorph taken from the Materials Project database[2], the average Si-O bond length differs from that of am-SiO_2 noticeably (see Table 1). This observation shows one of the possible limitations of the VAT model at the atomic level and possibly even for mesoporosity.

It is well known that SiO_2 has been used as gate material in the semiconductor industry for a long time. However, further reduction of the size of a transistor induces current leakage, which is attributed to direct tunneling of electrons through the SiO_2.[36] To solve the leakage problem, the dielectric constant of the gate material should be increased. Because of this, the computed results can be used as a simple guidance for modification of SiO_2 and design of new materials with desired dielectric constants. Moreover, although am-SiO_2 has a band gap energy too large for visible light absorption, the trends found here can illustrate the effect of amorphization on dielectric properties of materials. For instance, analysis of electronic properties clearly shows that amorphization induces the reduction of the difference between direct and indirect band gap affecting $\varepsilon_2(\omega)$ at low frequencies. This is similar to the observation for the crystalline-amorphous Si transition.[37, 38]

$\varepsilon(i\zeta)$ is another function which is often used in theoretical chemical physics especially to analyze the Lifshitz forces. Indeed, the understanding of volume dependence of

$\varepsilon(i\zeta)$ at atomic scale is of significant interest as the Lifshitz interaction (e.g. in multilayer membrane systems) and so called quantum levitation can be controlled by controlling $\varepsilon(i\zeta)$ of materials.[34, 35, 39-45] Studies of thin films on surfaces have clearly shown this effect.[44, 45] The fact that the Lifshitz force may change sign as separation increases has been explored by many groups following the initial work by Lifshitz and co-workers.[34, 39-43] Measurements of repulsive Lifshitz forces have also been reported in the literature.[46-49] In general, to model, analytically or numerically, van der Waals and Lifshitz forces, a very detailed knowledge of dielectric functions over a wide range of frequencies of all materials involved is essential. The details of the dielectric functions strongly influence colloidal interactions between charged surfaces in salt solutions.[50, 51]

Computing $\varepsilon(i\zeta)$ via the Kramers–Kronig relation $\varepsilon(i\zeta) = 1 + \frac{2}{\pi}\int_0^\infty d\omega \frac{\omega\varepsilon_2(\omega)}{\omega^2 + \zeta^2}$, it can be seen that, in contrast to real and imaginary part of the dielectric function at real frequencies, $\varepsilon(i\zeta)$ has smooth profile with a clear dependence at all frequencies. At low frequency limit ($\zeta \to 0$ eV), for semiconductors, according to the definition, $\varepsilon(i\zeta)$ has the same dependence as ε_∞. Indeed, for all frequencies, the dielectric function at imaginary frequencies has V^{-1} dependence. Moreover, the VAT model is still valid at all frequencies as $\varepsilon(i\zeta) = \frac{V_c}{V}\varepsilon_c(i\zeta) + 1 - \frac{V_c}{V}$. Based on this model, we can determine $\varepsilon_c^a(i\zeta)$ as the average $\varepsilon_c(i\zeta)$ of all considered am-SiO_2 structures. This function can describe $\varepsilon(i\zeta)$ of the am-SiO_2 samples with high accuracy (see Fig. 6a). Furthermore, the function can also be used to estimate $\varepsilon(i\zeta)$ for other phases having similar band gap energies. To illustrate this, we perform calculations for 6 different SiO_2 polymorphs found in the Materials Project database.[2] In Fig. 6b, we show that $\varepsilon(i\zeta)$ for all these materials can be accurately reproduced with a

parametrized $\varepsilon_c^a(i\zeta)$ and the VAT model (see Fig. 6b). To the best of our knowledge, this is the first observation of this kind at the atomic scale.

To apply the computed results for calculations of the Lifshitz forces and estimation of ε_∞, the parametrized $\varepsilon(i\zeta)$ is necessary. During the last years, a few different tabulated data for SiO_2 materials were reported.[34] However, even the most widely used $\varepsilon(i\zeta)$ results have noticeable difference. This is mainly because of limited experimental data. In this light, van Zwol and Palasantzas reported parametrization for two sets of dielectric functions[34] and indicated that the results found for different SiO_2 sets can have noticeable difference.[35] In general, $\varepsilon(i\zeta)$ can been represented as simple oscillator model with $\varepsilon(i\zeta) = 1 + \sum_j \frac{C_j}{1+(\zeta/\omega_j)^2}$, where C_j is the oscillator strength at given ω_j frequency. In this work, we limited our parametrization to a 4-order oscillator model. Herein we provide the data for $\varepsilon_c^a(i\zeta)$ only (see Table 2) as it can be used to reproduce $\varepsilon(i\zeta)$ for all materials discussed above using the VAT model. This means that, beside the single set of parameters for the master dielectric function, only zero frequency dielectric constants and the volumes need special attention as given in Table 1.

The Lifshitz force can be calculated accurately if the dielectric functions as a function of discrete imaginary frequencies for all media involved are known. Frequency intervals where the intervening medium has a dielectric permittivity in between the permittivity of the two interacting objects give a repulsive contribution; other intervals give an attractive contribution.[40-42] The transition from attractive to repulsive Lifshitz force occurs when attractive and repulsive frequency contributions exactly cancel. At this point even small changes in dielectric function of one of the media can have a dramatic effect on the transition distance. Take for instance an atomic force microscope tip of known dielectric properties interacting with a SiO_2 polymorph across a specific liquid. Then our simple expression for

dielectric functions of different SiO_2 polymorphs helps predicting how different nanoporosity can help fine tune the quantum levitation distance for a specific liquid by changing the SiO_2 polymorph. When the optical properties can be changed in a controlled manner there can be repulsion at predicted separations. Thus one can avoid problems with having too short quantum levitation distances where the surfaces would stick together by mechanical and chemical interactions. One can also explore the opposite direction. Tuning the materials to have repulsion when the surfaces are very close together will provide low friction devices where the two surfaces are in close proximity but via quantum levitation float on top of each other. Thus, the computed dependence is a simple guidance in the modification/search of materials with the desired dielectric properties.

Conclusions

Based on the first principles calculations, the analysis of dielectric and electronic properties of am-SiO_2 was performed. We found that the am-SiO_2 properties are volume dependent and the dependence is mainly caused by change of nanoporosity at the atomic scale. In particular, ε_∞ and $\varepsilon(i\zeta)$ of different am-SiO_2 samples can be accurately described using the expanded VAT model, Slater's atomic radii, and dielectric function of continuous media. Based on computed results, we show also that parametrized dielectric function of continuous media found for am-SiO_2 data and the VAT model can describe both ε_∞ and $\varepsilon(i\zeta)$ not only for am-SiO_2 but also for other SiO_2 polymorphs having similar band gap energies. Hence it is clear that the simple model described in this work can be used to identify specific materials having the desired dielectric properties.

Acknowledgments

The authors acknowledge the support from the Research Council of Norway (contract No. 221469). This work was performed on the Abel cluster, owned by the University of Oslo and the Norwegian Metacenter for Computational Science (NOTUR), and operated by the Department for Research Computing at USIT, the University of Oslo IT-department.

Supporting information

Additional results, details on computational methodology, and key structures are given as supporting information.

References

1. N. Binggeli, N. Troullier, J. L. Martins and J. R. Chelikowsky, *Phys. Rev. B*, 1991, 44, 4771-4777.
2. A. Jain, S. P. Ong, G. Hautier, W. Chen, W. D. Richards, S. Dacek, S. Cholia, D. Gunter, D. Skinner, G. Ceder and K. A. Persson, *APL Mat.*, 2013, 1, 011002.
3. S. T. Pantelides and W. A. Harrison, *Phys. Rev. B*, 1976, 13, 2667-2691.
4. F. Messina, E. Vella, M. Cannas and R. Boscaino, *Phys. Rev. Lett.*, 2010, 105, 116401.
5. J. Sarnthein, A. Pasquarello and R. Car, *Phys. Rev. Lett.*, 1995, 74, 4682-4685.
6. R. M. Van Ginhoven, H. Jónsson and L. R. Corrales, *Phys. Rev. B*, 2005, 71, 024208.
7. D. Zhao, J. Feng, Q. Huo, N. Melosh, G. H. Fredrickson, B. F. Chmelka and G. D. Stucky, *Science*, 1998, 279, 548-552.
8. M. Vallet-Regi, L. Ruiz-Gonzalez, I. Izquierdo-Barba and J. M. Gonzalez-Calbet, *J. Mater. Chem.*, 2006, 16, 26-31.
9. H. Ni, X. Li and H. Gao, *Appl. Phys. Lett.*, 2006, 88, 043108.

10. J. N. Cha, G. D. Stucky, D. E. Morse and T. J. Deming, *Nature*, 2000, 403, 289-292.

11. L. Martin-Samos, G. Bussi, A. Ruini, E. Molinari and M. J. Caldas, *Phys. Status Solidi B*, 2011, 248, 1061-1066.

12. M. Benoit, S. Ispas, P. Jund and R. Jullien, *Eur. Phys. J. B*, 2000, 13, 631-636.

13. D. Donadio, M. Bernasconi and F. Tassone, *Phys. Rev. B*, 2003, 68, 134202.

14. L. Giacomazzi, P. Umari and A. Pasquarello, *Phys. Rev. B*, 2009, 79, 064202.

15. J. P. Perdew, K. Burke and M. Ernzerhof, *Phys. Rev. Lett.*, 1996, 77, 3865.

16. G. Kresse and D. Joubert, *Phys. Rev. B*, 1999, 59, 1758-1775.

17. P. E. Blöchl, *Phys. Rev. B*, 1994, 50, 17953-17979.

18. H. J. Monkhorst and J. D. Pack, *Phys. Rev. B*, 1976, 13, 5188-5192.

19. S. Nosé, *J. Chem. Phys.*, 1984, 81, 511-519.

20. D. M. Bylander and L. Kleinman, *Phys. Rev. B*, 1992, 46, 13756-13761.

21. M. Gajdoš, K. Hummer, G. Kresse, J. Furthmüller and F. Bechstedt, *Phys. Rev. B*, 2006, 73, 045112.

22. X. Wu, D. Vanderbilt and D. R. Hamann, *Phys. Rev. B*, 2005, 72, 035105.

23. T. Tamura, S. Ishibashi, S. Tanaka, M. Kohyama and M. H. Lee, *Phys. Rev. B*, 2008, 77, 8.

24. T. H. DiStefano and D. E. Eastman, *Solid State Commun.*, 1971, 9, 2259-2261.

25. V. Fiorentini and A. Baldereschi, *Phys. Rev. B*, 1995, 51, 17196-17198.

26. M. Harb, P. Labéguerie, I. Baraille and M. Rérat, *Phys. Rev. B*, 2009, 80, 235131.

27. G. Ghosh, *Opt. Commun.*, 1999, 163, 95-102.

28. J. Kischkat, S. Peters, B. Gruska, M. Semtsiv, M. Chashnikova, M. Klinkmüller, O. Fedosenko, S. Machulik, A. Aleksandrova, G. Monastyrskyi, Y. Flores and W. Ted Masselink, *Appl. Opt.*, 2012, 51, 6789-6798.

29. M. M. Braun and L. Pilon, *Thin Solid Films*, 2006, 496, 505-514.

30. A. Garahan, L. Pilon, J. Yin and I. Saxena, *J. Appl. Phys.*, 2007, 101, 014320.

31. A. Navid and L. Pilon, *Thin Solid Films*, 2008, 516, 4159-4167.

32. J.-Y. Noh, H. Kim and Y.-S. Kim, *Phys. Rev. B*, 2014, 89, 205417.

33. J. C. Slater, *J. Chem. Phys.*, 1964, 41, 3199-3204.

34. P. J. van Zwol and G. Palasantzas, *Phys. Rev. A*, 2010, 81, 062502.

35. P. J. van Zwol, G. Palasantzas and J. T. M. De Hosson, *Phys. Rev. B*, 2009, 79, 195428.

36. J. Robertson, *Eur. Phys. J. Appl. Phys.*, 2004, 28, 265-291.

37. A. V. Shah, H. Schade, M. Vanecek, J. Meier, E. Vallat-Sauvain, N. Wyrsch, U. Kroll, C. Droz and J. Bailat, *Prog. Photovolt. Res. Appl.*, 2004, 12, 113-142.

38. D. E. Carlson and C. R. Wronski, *Appl. Phys. Lett.*, 1976, 28, 671-673.

39. I. E. Dzyaloshinskii, E. M. Lifshitz and L. P. Pitaevskii, *Adv. Phys.*, 1961, 10, 165-209.

40. B. W. Ninham and V. A. Parsegian, *Biophys. J.*, 1970, 10, 646-663.

41. P. Richmond and B. W. Ninham, *Solid State Commun.*, 1971, 9, 1045-1047.

42. P. Richmond, B. W. Ninham and R. H. Ottewill, *J. Colloid Interface Sci.*, 1973, 45, 69-80.

43. M. Boström, B. E. Sernelius, I. Brevik and B. W. Ninham, *Phys. Rev. A*, 2012, 85, 010701.

44. C. H. Anderson and E. S. Sabisky, *Phys. Rev. Lett.*, 1970, 24, 1049-1052.

45. F. Hauxwell and R. H. Ottewill, *J. Colloid Interface Sci.*, 1970, 34, 473-479.

46. J. N. Munday, F. Capasso and V. A. Parsegian, *Nature*, 2009, 457, 170-173.

47. A. Milling, P. Mulvaney and I. Larson, *J. Colloid Interface Sci.*, 1996, 180, 460-465.

48. S.-w. Lee and W. M. Sigmund, *J. Colloid Interface Sci.*, 2001, 243, 365-369.

49. A. A. Feiler, L. Bergström and M. W. Rutland, *Langmuir*, 2008, 24, 2274-2276.

50. M. Boström, D. R. M. Williams and B. W. Ninham, *Phys. Rev. Lett.*, 2001, 87, 168103.

51. D. F. Parsons, M. Boström, P. L. Nostro and B. W. Ninham, *Phys. Chem. Chem. Phys.*, 2011, 13, 12352-12367.

Table 1 Volume per SiO_2 unit (V, in $Å^3$), average Si-O bond length (d, in Å), band gap energy (E_g, in eV), high frequency dielectric constant with scissors-operator correction (ε_∞), ionic contribution (χ) to the dielectric constant, and static dielectric constant (ε_0)

V	d	E_g	ε_∞	χ	ε_0
am-SiO_2					
41.14	1.634	5.16	2.184	2.140	4.323
41.44	1.635	5.22	2.177	1.992	4.169
41.80	1.636	5.30	2.169	1.984	4.153
42.48	1.636	5.28	2.149	1.917	4.066
43.17	1.634	5.27	2.126	1.908	4.034
43.31	1.633	5.33	2.122	1.880	4.002
43.60	1.633	5.35	2.113	1.867	3.980
44.09	1.635	5.31	2.108	1.850	3.957
44.30	1.631	5.43	2.091	1.822	3.913
44.53	1.634	5.45	2.090	1.805	3.896
SiO_2 polymorphs					
23.66	1.800	5.24	3.007	8.126	11.133
35.68	1.630	5.54	2.357	2.609	4.966
56.96	1.621	5.39	1.831	1.427	3.257
68.82	1.643	5.20	1.724	0.913	2.636
106.39	1.657	5.35	1.476	0.365	1.841
141.87	1.652	5.67	1.347	0.344	1.691

Table 2 Parametrization of average dielectric function of continuous media ($\varepsilon_c^a(i\zeta)$) at imaginary frequencies used in the VAT model. Here V_c is the sum of atomic volumes for one Si and two O atoms computed using the Slater's atomic radii ($V_c = 7.381$ Å^3)[33]

	mode 1	mode 2	mode 3	mode 4
C_j	2.111	3.531	0.831	0.119
ω_j	12.579	18.555	32.937	67.335

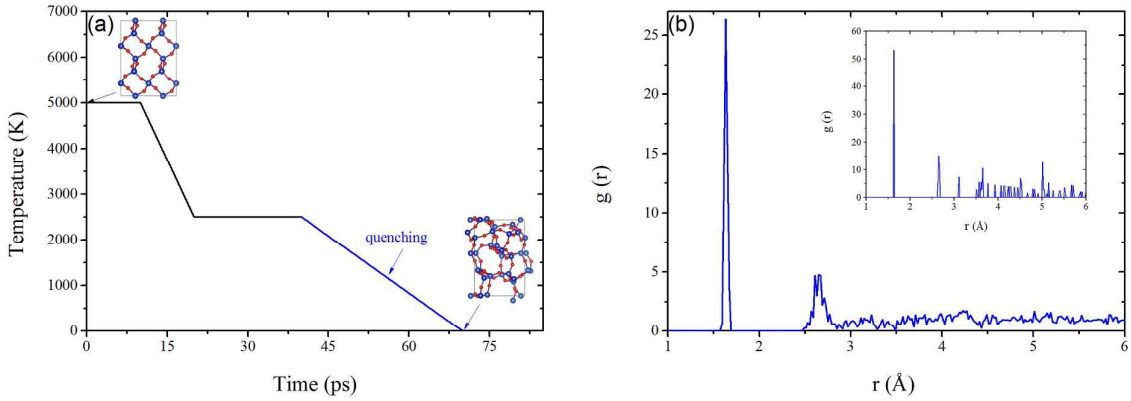

Figure 1 (a) Schematic illustration of typical temperature protocol used to generate the am-SiO_2 samples. The structures represent the typical initial α-SiO_2 and fully optimized am-SiO_2 structures. (b) Typical radial distribution function ($g(r)$) of fully optimized am-SiO_2. The inset shows $g(r)$ for α-SiO_2.

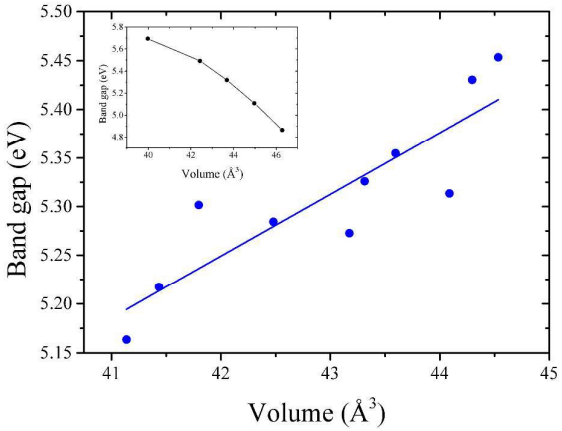

Figure 2 Band gap energies of the am-SiO_2 samples as a function of volume per SiO_2 unit. The blue line represents the fitted function. The inset shows the band gap energies for α-SiO_2 as a function of the volume. The black line is a guide for the eye.

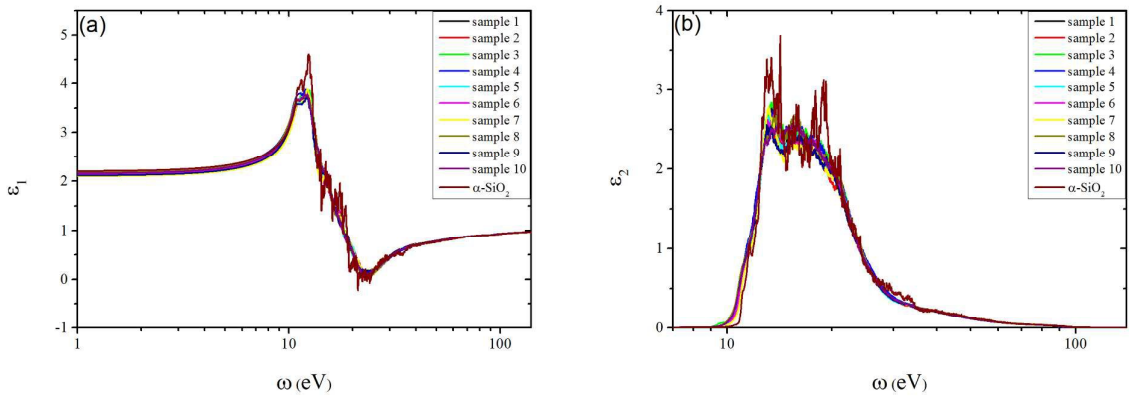

Figure 3 (a) Real and (b) imaginary parts of the dielectric functions for α-SiO_2 and am-SiO_2 samples computed using the scissors-operator approximation with $\Delta = 3.6$ eV.

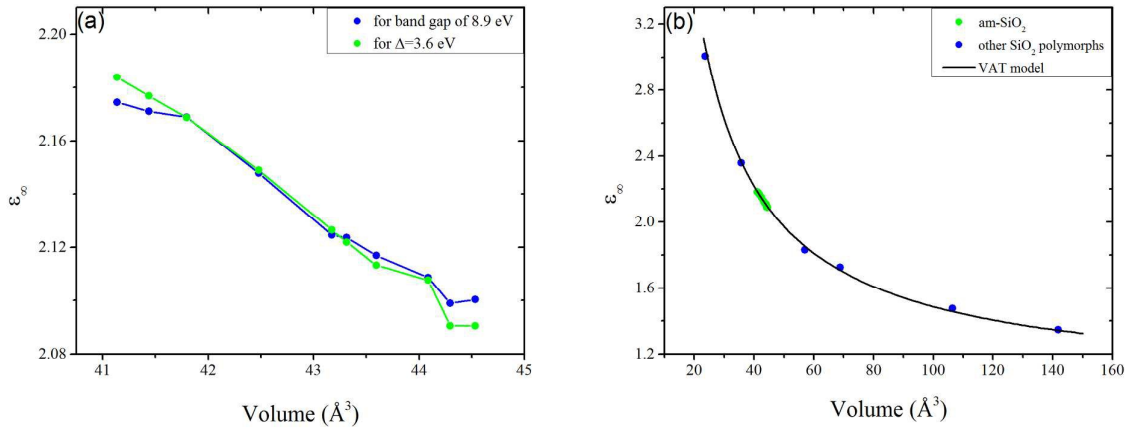

Figure 4 (a) High frequency dielectric constant (ε_∞) as a function of volume per SiO_2 unit. The results are shown for different values of scissors-operators (Δ). The green dots correspond to the values computed for Δ = 3.6 eV. The blue dotes correspond to the results computed with band gap energies tuned to 8.9 eV for each sample. The lines are a guide for the eye. (b) The VAT extrapolation of ε_∞ dependence found for am-SiO_2 samples. The green points represent ε_∞ for different am-SiO_2 samples, while the blue points are ε_∞ of other SiO_2 polymorphs. For all systems, Δ = 3.6 eV.

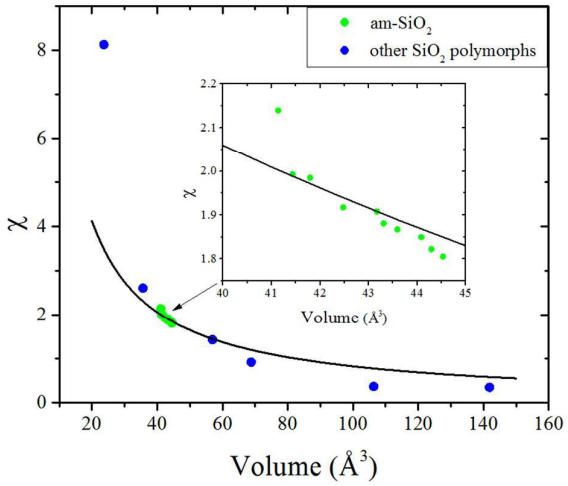

Figure 5 Ionic contribution (χ) to static dielectric constant of SiO_2 polymorphs as a function of volume per SiO_2 unit. Black line is inverse volume (V^{-1}) extrapolation of the am-SiO_2 data. The green points represent the ionic contributions to the dielectric constants of the am-SiO_2 samples, while the blue points are the data for other SiO_2 polymorphs.

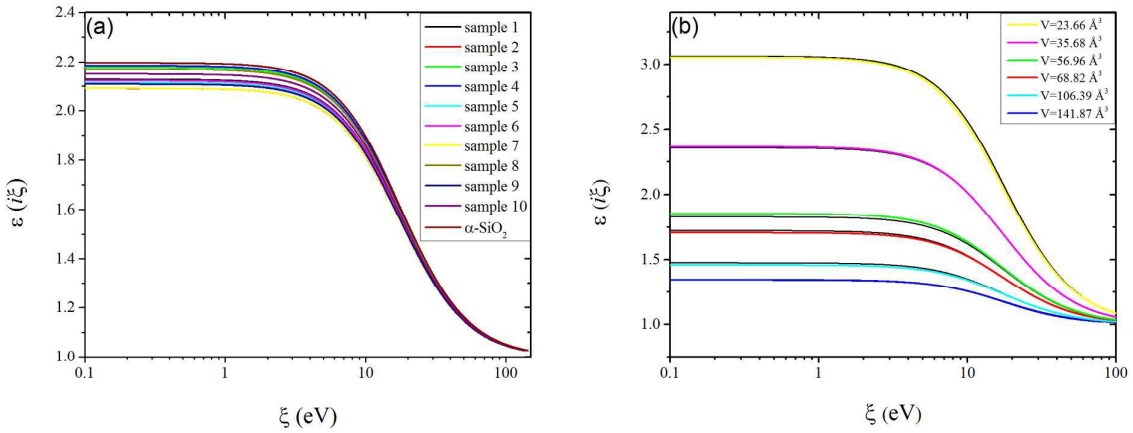

Figure 6 (a) Dielectric functions at imaginary frequencies ($\varepsilon(i\zeta)$) for the am-SiO_2 samples. (b) $\varepsilon(i\zeta)$ for different SiO_2 polymorphs. The color and black lines represent the computed data and the VAT extrapolation of am-SiO_2 data, respectively. For all systems, the ionic contribution to the dielectric function is not shown and $\Delta = 3.6$ eV.